Clim Dyn
DOI 10.1007/s00382-012-1326-z

Analysis of the long-term surface wind variability over complex terrain using a high spatial resolution WRF simulation

Pedro A. Jiménez · J. Fidel González-Rouco · Juan P. Montávez · E. García-Bustamante · J. Navarro · J. Dudhia

Received: 9 January 2012 / Accepted: 24 February 2012

Abstract This work uses a WRF numerical simulation from 1960 to 2005 performed at a high horizontal resolution (2 km) to analyze the surface wind variability over a complex terrain region located in northern Iberia. A shorter slice of this simulation has been used in a previous study to demonstrate the ability of the WRF model in reproducing the observed wind variability during the period 1992–2005. Learning from that validation exercise, the extended simulation is herein used to inspect the wind behavior where and when observations are not available and to determine the main synoptic mechanisms responsible for the surface wind variability. A principal component analysis was applied to the daily mean wind. Two principal modes of variation accumulate a large percentage of the wind variability (83.7%). The first mode reflects the channeling of the flow between the large mountain systems in northern Iberia modulated by the smaller topographic features of the region. The second mode further contributes to stress the differentiated wind behavior over the mountains and valleys. Both modes show significant contributions at the higher frequencies during the whole analyzed period, with different contributions at lower frequencies during the different decades. A strong relationship was found between these two modes and the zonal and meridional large scale pressure gradients over the area. This relationship is described in the context of the influence of standard circulation modes relevant in the European region like the North Atlantic Oscillation, the East Atlantic pattern, East Atlantic/Western Russia pattern, and the Scandinavian pattern.

Keywords Surface wind variability · Dynamical downscaling · WRF · Multivariate analysis

P. A. Jiménez (✉) · J. F. González-Rouco
Departamento de Astrofísica y CC, de la Atmósfera,
Faculatad de CC, Físicas, UCM,
Avenida Complutense s/n, 28040 Madrid, Spain
e-mail: pedro.jimenez@fis.ucm.es

P. A. Jiménez · J. Navarro
División de Energías Renovables, CIEMAT,
28040 Madrid, Spain

J. P. Montávez
Departamento de Física, Universidad de Murcia,
Murcia, Spain

E. García-Bustamante
Department of Geography,
Justus-Liebig University of Giessen,
Giessen, Germany

J. Dudhia
Mesoscale and Microscale Meteorology Division,
NCAR, Boulder, CO, USA

1 Introduction

The long-term wind variability is an issue of relevance not only from the academic point of view but also for several applications such as the wind insurance industry, transport and dispersion of pollutants, decision making in high risk situations such as forest fires, etc. An important emphasis has been made to analyze the wind speed trends (e.g. Klink 1999, 2002; Pryor and Barthelmie 2003; Xu et al. 2006; McVicar et al. 2008, 2010; Pryor et al. 2009, Pryor and Ledolter 2010; Vautard et al. 2010; Wan et al. 2010; Guo et al. 2011) or the wind speed variability (e.g. Palutikof et al. 1987; Archer and Jacobson 2003, 2004; Klink 2007; George and Wolfe 2009; Davy et al., 2010; He et al. 2010; Rahimzadeh et al. 2011; Martín et al. 2011). Dealing with the wind as a scalar variable allows to acquire certain

Published online: 08 March 2012

understanding of the long-term behavior of the flow. However, it presents the drawback of loosing information regarding wind direction.

Understanding the wind variability is especially challenging over complex terrain regions. The observational networks over these areas need a reasonably high density of spatial sampling in order to adequately represent the most important characteristics of the flow. These kinds of networks have proliferated with the advent of automated weather stations (Horel et al. 2002) and have allowed us to study certain characteristics of the regional flow (e.g. Kaufmann and Weber 1996; Kaufmann and Whiteman 1999; Ludwig et al. 2004; Burlando et al. 2008; Jiménez et al. 2008, 2009a, b). For instance, Jiménez et al. (2008, JEA08 hereafter) analyzed the wind variability over a complex terrain region using observations from 1992 to 2002, thereby evidencing the strong influence that the orography produces over the surface circulations. Unfortunately, the time span of observational networks in case studies like that of JEA08 is often limited to a few years or decades (e.g. Burlando et al. 2008) and does not allow for exploring low frequency, even multi-decadal, wind variability. This limitation can be partially mitigated by using numerical simulations that are longer than the observational records and with spatial resolutions that can also reduce potential uncertainties associated with insufficient spatial coverage of the observational networks (PaiMazumder and Mölders 2009). Such simulations can be compared with the available observations in order to evaluate their ability to reproduce the behavior of the observed wind (e.g. Buckley 2004; Rife et al. 2004, 2009; Rife and Davis 2005; Zagar et al. 2006; Jiménez et al. 2010a). For instance, Hughes and Hall (2010) used a mesoscale simulation to understand the mechanisms causing the California's Santa Ana winds once the ability of the simulation to reproduce the observed wind behavior was confirmed. In order to have the best possible representation of the topography it is desirable that high spatial resolution is used. In addition, if long temporal periods are targeted this makes these kinds of numerical experiments scarce and still challenging in terms of computational resources. Promising results were recently found by Jiménez et al. (2010a, JEA10a hereafter) that have shown the ability of a simulation performed with the Weather Research and Forecasting model (WRF, Skamarock et al. 2005) configured at high horizontal resolution (2 km) to reproduce the observed wind variability over the period 1992–2005 in the same region described by JEA08.

This study extends the WRF dynamical downscaling described in JEA10a to the period from 1960 to 2005 and analyzes the local/regional wind variability over the area beyond the limits allowed by observations. The high spatial resolution used and the extended simulated period allows for investigating the wind variability at time scales comparable to reanalyses products (Uppala et al. 2005; Kalnay et al. 1996) but at much finer spatial scales. Our research is based on principal component analysis (PCA) applied to the wind components and thus, information regarding the flow direction is taken into account. The PCA is applied to the daily wind time series in order to mitigate the influence of the intradiurnal circulations and thus concentrate the investigation on the influence that the interaction between the synoptic circulation and topography produces on the surface wind. The main modes of variation are retained and analyzed in order to understand the spatio-temporal wind variability. On the basis of the good performance of the simulation to reproduce the temporal variability, the principal components (PCs) are further used to understand the main synoptic forcings responsible for the long-term wind variability. The long simulated period (over 45 years) allows to robustly determine these connections.

The rest of the manuscript is organized as follows. The next section describes the WRF dynamical downscaling. Section 3 analyzes the spatio-temporal variability of the wind over the region whereas Sect. 4 explores the large scale mechanisms responsible for the regional wind variability. Finally, a summary and the conclusions are presented in Sect. 5.

2 WRF dynamical downscaling

The region of study is the Comunidad Foral de Navarra (CFN), a complex terrain region located in the northeast of the Iberian Peninsula (Fig. 1). The northern areas show more complicated topography than the southern ones that are dominated by the low lands of the Ebro valley (see zoomed area in Fig. 1). The western areas are dominated by the presence of the small sierras of Aralar, Andia, Urbasa and Santiago. To simplify, the later will be referred to as the *western mountains*, unless treated specifically. To the North, the mountain lines of Bidasoa, Abodi, Uztarroz, Zariqueta and San Miguel form the last foothills of the Pyrenees and will be labeled as the *northern mountains*. Central areas are dominated by the sierra of Izco and the Ujué Peak which are labeled as the *central mountains*. The sierras of Leyre and San Pedro outflank the eastern areas of the CFN and will be referred to as the *eastern mountains*. The system of sierras that constitute the *western, central* and *eastern mountains* act as the northern boundary of the Ebro valley over the CFN which is limited to the South by the Iberian system.

The extension of the dynamical downscaling follows JEA10a. A total of four domains are configured in two way nesting in order to reach a horizontal resolution of 2 km over the innermost domain that covers the whole CFN

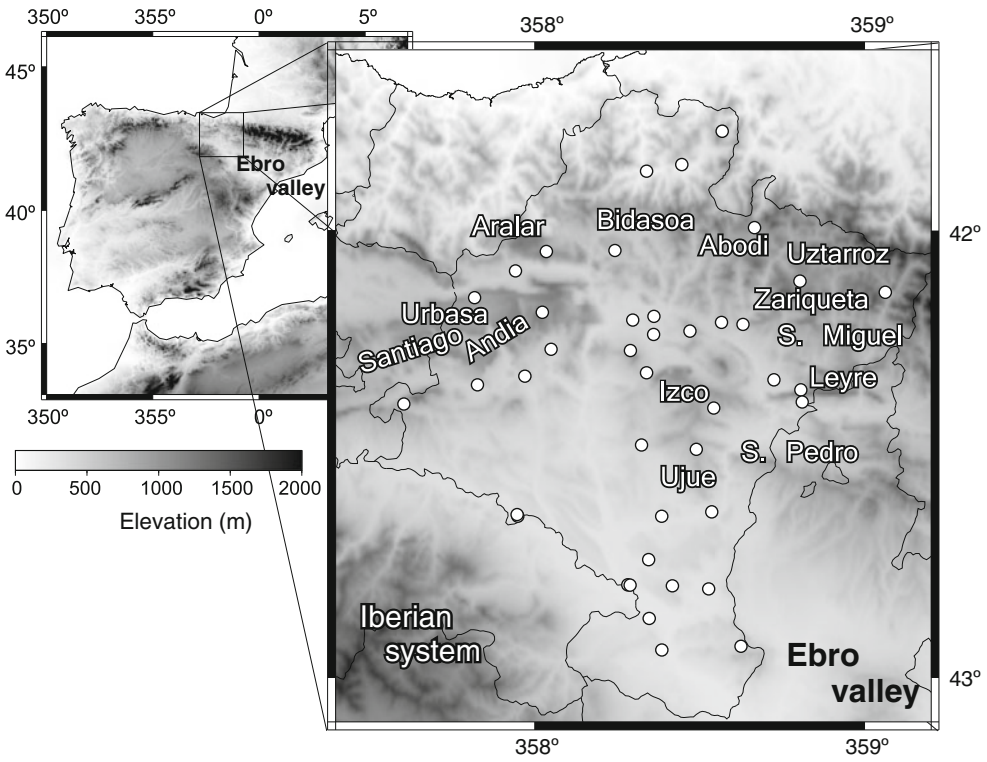

Fig. 1 Location of the CFN within the Iberian Peninsula. The *zoomed area* shows the topographic details of the CFN (*shaded*) as well as the location of the observational sites (*circles*). The main topographic features are *highlighted* (modified from JEA08)

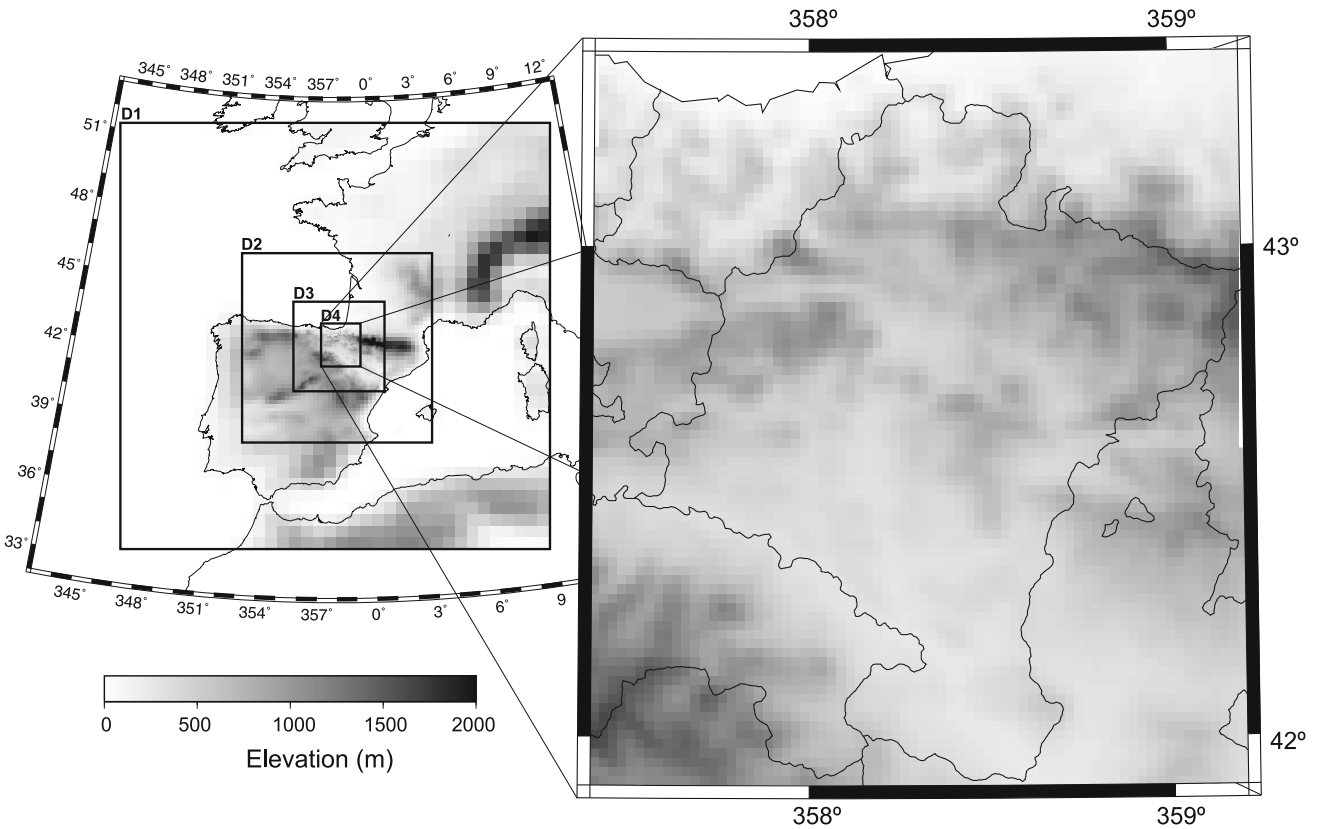

Fig. 2 Spatial configuration of the domains used in the WRF simulation. The topography of each domain is displayed at its specific horizontal resolution, 54 km (*D1*), 18 km (*D2*), 6 km (*D3*) and 2 km (*D4*). The *zoomed area* highlights the topography used in *D4* over the region under study (see *zoomed area* in Fig. 1)

(Fig. 2). The high horizontal resolution used is necessary to realistically represent in the downscaling the different sierras and valleys that characterize the topographic features of the CFN (see zoomed area in Fig. 2). The downscaling consists of a sequence of concatenated short WRF runs since this has been shown to provide better comparison with observations than a long continuous simulation (e.g. Lo et al. 2008). The model is initialized at the 0 h of a given day and it is run for 48 h recording the output every hour. The first 24 h are discarded as a spin up of the simulation, and the second 24 h are retained and averaged to obtain the simulation for that day. The process is repeated until obtaining a WRF simulation for all the days from 1960 to 1991. Data from the ERA-40 reanalysis project ($1 \times 1°$) performed at the European Center for Medium-Range Weather Forecast (ECMWF, Uppala et al. 2005) is used as initial and boundary conditions. See JEA10a for further details in the dynamical and physical settings of the downscaling.

JEA10a found that the WRF simulation at 2 km of horizontal resolution is able to reproduce the spatio-temporal wind variability over the area (JEA08), showing a clear added value with respect to the ECMWF data used as initial and boundary conditions (ERA-40 before August 2002 and the ECMWF operational analysis afterwards). The good performance at the 41 observational sites (circles in Fig. 1) motivated its extension in this work in order to cover the 1960–2005 period. The extended simulation provides both a much longer temporal coverage than the observations (1992–2005, Jiménez et al. 2010b) and a much higher spatial sampling, since the innermost domain is configured with 90 by 96 grid points and thus wind information is available at a total of 8,640 grid points (instead of the 41 observational sites). The extended simulation is herein used to provide a statistically robust characterization of the spatio-temporal wind variability over the region and its main synoptic forcing mechanisms. Although JEA10a provided an extensive evaluation of the downscaling performance, some complementary information will be herein shown in order to further illustrate the ability of the downscaling to reproduce the surface wind variability.

3 Regional wind variability

The wind variability is investigated by applying PCA to the correlation matrix of the daily mean wind components at 10 m above ground level. Hence, the PCA is applied jointly to both wind components as it was done in JEA08 and JEA10a. The presence of an annual cycle in the surface circulations (JEA08) led to compute the wind anomalies by subtracting this deterministic behavior. This allows us to concentrate in the variability and therefore avoid any kind of systematic biases that the simulation may present (e.g. Jiménez and Dudhia 2012). Wind information at the 8,640 grid points of the innermost WRF domain is used in the PCA. Performing the analysis with daily means mitigates the influence of the intradiurnal variability and therefore avoids the limitations that WRF presents to reproduce it at certain locations (Jiménez et al. 2009b). The investigation is therefore concentrated on the influence that the large scale atmospheric variability and its interaction with topography exerts on the surface flow.

The first two main modes of variation account for 83.7% of the variance (the first 57.1% and the second 26.6%, Table 1). The third mode accounts for much lower variance (3.0%). These numbers are in good agreement with those shown by a PCA applied to the daily wind at the 41 observational sites (second column in Table 1). The observations reveal however a larger contribution of the first mode in detriment of the second one, but this is a consequence of the smaller sampling of mountain areas where it will be herein shown that the second mode shows larger loads. Indeed, when we applied PCA to the simulated wind at the 41 observational sites the variance explained by the first modes is in better agreement with observations. The first mode explains 71.4% of the variance and the second one 17.9%. Hence, the discrepancy with respect to the first (second) observational mode was reduced from 9.2% (17.1%) to 5.1% (8.4%).

On the basis of these considerations, the first two modes of variation are retained for analysis. The next sections describe the spatial (Sect. 3.1) and temporal (Sect. 3.2) variability of these modes.

3.1 Spatial variability

The first and second empirical orthogonal functions (EOFs) renormalized by the standard deviation to provide units to the vectors are shown in Figs. 3 and 4, respectively. The loads from the WRF simulation (black arrows) are in agreement with the loads from the observations (white arrows) providing further evidence of the dynamical downscaling ability to reproduce the regional wind variability. However, some discrepancies can be noticed. WRF shows a tendency to overestimate the wind in the valleys

Table 1 Percentage of variance accounted for by the three main principal modes of variation calculated with WRF and the observations

	WRF (1960–2005)	Obs. (1992–2005)
First mode	57.1	66.3
Second mode	26.6	9.5
Third mode	3.0	3.6

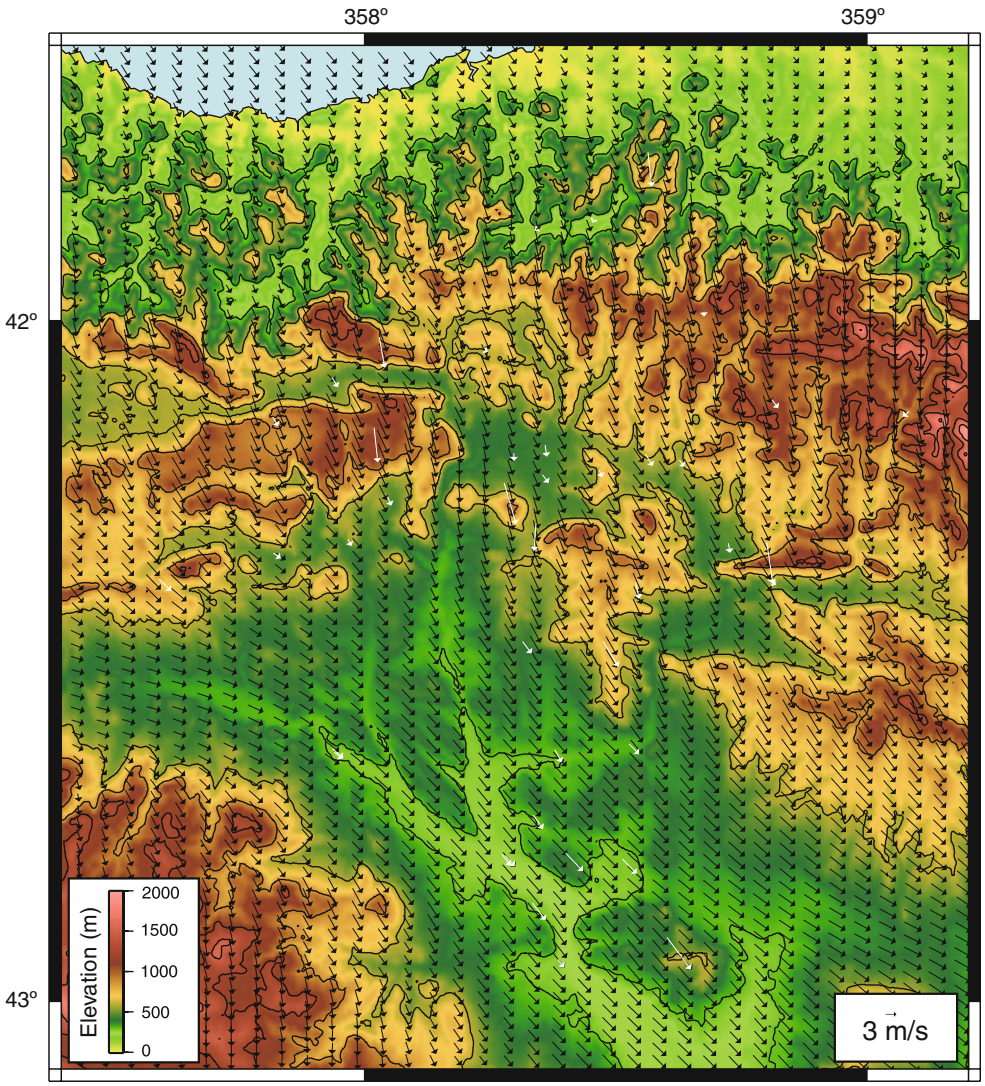

Fig. 3 First renormalized EOF calculated with the WRF simulation that covers the 1960–2005 period (*black arrows*) and with the observations that span the 1992–2005 period (*white arrows*). For illustrative purposes, only one of every two grid points of the WRF grid are represented. The topography is also shown (*shaded*)

and to underestimate it in the mountains. This is a result of the renormalization, since WRF presents these kinds of biases in the wind speed (Jiménez and Dudhia 2012) and both variables, the mean wind speed and its standard deviation, are correlated (r = 0.98, JEA08). The interpretation becomes more evident calculating the scalar product between the first two eigenvectors from PCA calculated with WRF and the observations at the 41 observational sites (Table 2). A high degree of orthonormality is evidenced. The first (second) eigenvectors show a scalar product of 0.95 (0.89) whereas the product between them is near zero (0.12 and −0.12). The scalar product between the 41 nearest vectors to the observational sites from Figs. 3 and 4, renormalized to have a unit length, and the eigenvectors from the observations shows nearly the same values shown in Table 2. The high degree of orthonormality reveals the ability of the simulation to reproduce the spatial variability of the modes, and indicates that the discrepancies that we can appreciate in Figs. 3 and 4 arise mostly from the renormalization of the EOFs. Results also indicate that WRF is in somewhat better agreement with the first mode than with the second one.

The first EOF displays northwestern (southeastern) circulations over the Ebro valley in its positive (negative) phase. For the sake of brevity only the positive phase will be described but analogous arguments can be used to explain its negative counterpart. The circulations from northern areas of the CFN are split by the *western mountains* and the flow penetrates into the Ebro valley from the east in its western flank and from the North in its eastern flank. The main channeling occurs between the *northern* and *western mountains* just to the north of Aralar and over the mountain line of Bidasoa (see the zoomed in area in Fig. 1 for the location of these topographical features), wherein the terrain elevations are not as high as the surrounding sierras. The splitting of the flow around the *central mountains* is also noticeable. The wind anomalies show a more meridional orientation at the highest

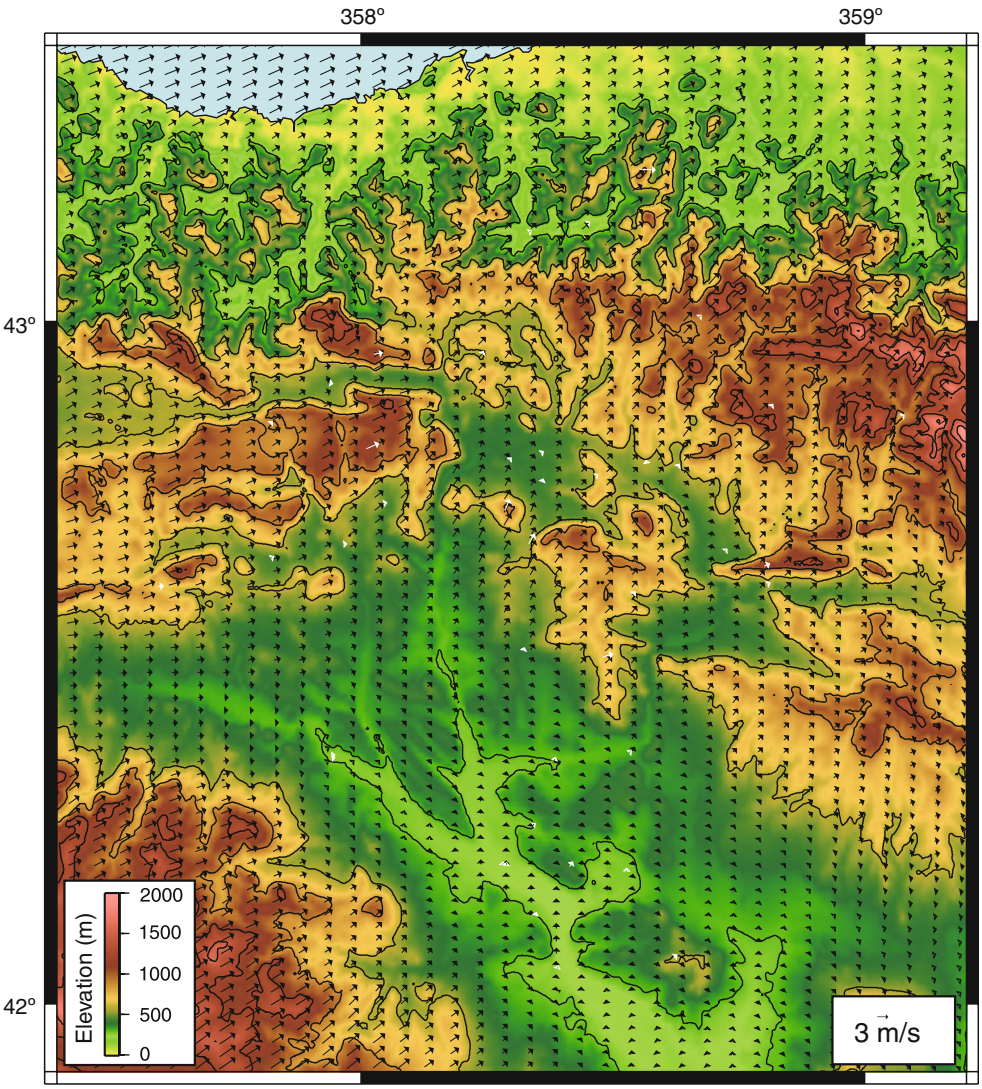

Fig. 4 Same as Fig. 3 but for the second EOF

Table 2 Scalar product between the first two eigenvectors from PCA applied to the simulated and observed wind at the 41 observational sites during the observational period (1992–2005)

	Eigenvector 1 (WRF)	Eigenvector 2 (WRF)
Eigenvector 1 (obs.)	0.95	0.12
Eigenvector 2 (obs.)	−0.12	0.89

elevations such as the *northern mountains* or the Iberian system in the South indicating a certain decoupling of the flow from the surface circulations over the valleys. This mode can be interpreted as the influence exerted by the main mountain systems in northern Iberia (Fig. 1) that in the positive (negative) phase channel the flow down (up) the Ebro valley.

The second EOF shows southwestern (northeastern) circulations in its positive (negative) phase (Fig. 4). The highest loads appear over the highest mountains such as the Iberian system, the *northern mountains* over the Pyrenees or the *western mountains*. Less intense flow is evidenced over the *central mountains* and the *eastern mountains*. The low lands of the Ebro valley show a weak southwestern flow that is channeled to northern areas around the *central mountains*. Higher loads over the valleys located in northern areas of the CFN can be recognized. The mode represents the larger influence that the synoptic circulation exerts over the higher locations.

Keeping aside the limitations to reproduce the standard deviation of the wind, the good agreement between the observed and simulated EOFs (Figs. 3, 4) indicates that the limited number of observational sites is able to discern the main modes of variability over the region. Note that the observations and the simulation not only differ in the spatial resolution but also in the temporal coverage. The two EOFs are therefore robustly defined during the over 45 year period spanned by the simulation (1960–2005). This result goes further beyond to what can be obtained

with the reduced temporal coverage of the observational network (1992–2005) or even with the simulation of JEA10a since it covers the same temporal period. The good replication of the spatial variability of the patterns can be interpreted as an added value of the simulation with respect to the ECMWF data used as initial and boundary conditions since the coarser horizontal resolution of the latter (1°) is unable to provide details of the flow over the region.

3.2 Temporal wind variability

The two PCs associated with the main modes of variation (Figs. 3, 4) are shown in Fig. 5. For illustrative purposes the time series shown are filtered using a 60-day moving average, but the correlations shown are computed using the daily time series. Both PCs from the WRF downscaling are in good agreement with the PCs calculated with observations ($r = 0.87$ and 0.72 for the first and second mode respectively). Notice that a perfect agreement should not be expected since the WRF PCA was calculated using information at the 8640 grid points of the simulated grid whereas the observations consist of the time series at the 41 observational sites. Actually, the correlations are increased when only the simulated wind at the 41 observational sites is considered, although this increase is slight for the first PC ($r = 0.89$) and moderate for the second one ($r = 0.79$). The good concordance between the PCs during the observational period provides more reliability to the dynamical downscaling before 1992 when no observations are available.

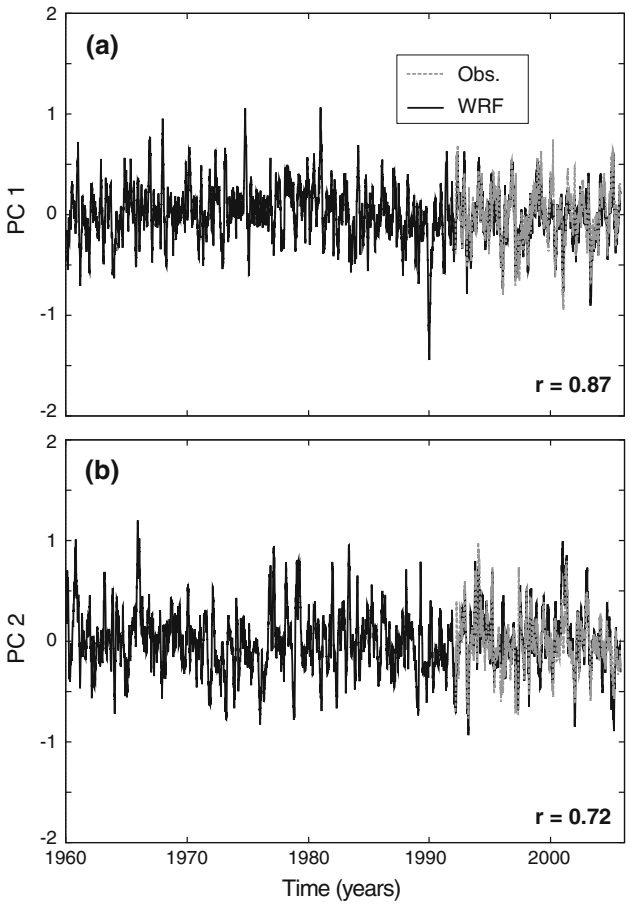

Fig. 5 The 60-day moving average filter outputs of the PCs of the main modes of variation shown in Figs. 3 and 4. The correlation between the unfiltered PCs (daily resolution) is also shown

The PCs do not show noticeable trends or important changes in the variability of the time series (Fig. 5). Hence, low frequency variations play a secondary role in controlling the wind behavior over the CFN during 1960–2005. This important finding highlights the advantages of the extended simulation to complement the observational and numerical investigations during 1992–2005 (JEA08, JEA10a), since no information of the decadal variability could had been obtained given the reduced temporal period. The end of the 1970s and the beginning of the 1980s are the periods with stronger northwestern anomalies in the positive phase of the first mode (Fig. 5a). The largest anomalous wind was however from the southeast in December 1989. PC2 shows a dominance of the northeastern winds of the negative phase at the beginning of the 1970s but changes to positive at the end of the decade (Fig. 5b). The maximum anomaly occurs in December 1965 and contributes to the positive phase. A certain decadal variability can be recognized in this second mode of variation.

Complementary information of the temporal variability of the modes is obtained calculating the wavelet spectra (Torrence and Compo 1998) of the PCs (Fig. 6). Both wavelet spectra present significant activity at the synoptic scale (periods lower than 10 days) but with different contributions at lower frequencies. The first mode shows a tendency to increase the periods of the significant contributions of the low frequency variations from 100 to 500 days (about 2 years) (Fig. 6a). It shows an important band around periods of 2,500 days (about 6 or 7 years) but is only significant during the second half of the 1980s and the beginning of the 1990s. The second mode shows less activity between 100 and 500 days (about 2 years) (Fig. 6b). The bands with significant activity are displaced towards periods between 500 and 1,000 days (about 2 and 3 years) in the 1960s and 1990s but they are close to the cone of influence where the effects of the edges become important. The band at lower frequencies does not appear in this case.

4 Large scale influence on the regional wind

The relationship between the synoptic situation and the regional wind variability is inspected by calculating the correlation maps between the PCs of the wind (Fig. 5) and

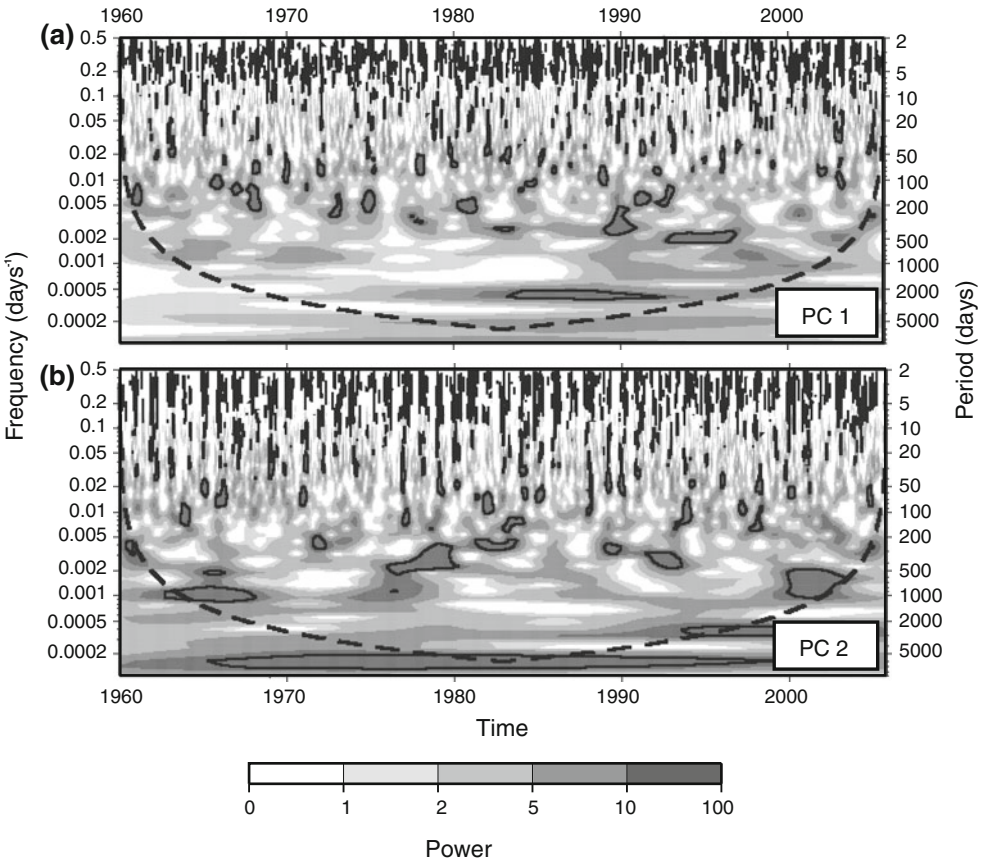

Fig. 6 Wavelet spectral power of the first (**a**) and second (**b**) PCs from the WRF simulation. The *shaded areas* represent normalized variances higher than 1, 2, 5, and 10 whereas the *black thick contour lines* enclose regions of confidence above 95% for the first-order auto-regressive process. The *dashed line* represent the "cone of influence", below which edge effects become important (Torrence and Compo 1998)

the daily mean sea level pressure (SLP) fields from the ECMWF data used as initial and boundary conditions for the dynamical downscaling (Sect. 4.1). Further exploration of the influence exerted by the large scale is investigated through the analysis of the relationship between the PCs and circulation indexes such as those of the main teleconnection patterns over the North Atlantic area (Sect. 4.2). The long simulated period, 45 years, allows to robustly characterize these relationships.

4.1 Sea level pressure

The correlation maps between the SLP and the PCs of the regional wind are shown in Fig. 7. The first mode shows a positive center of correlation over the Atlantic ocean and a negative one to the north of Italy (Fig. 7a). A reinforcement of the Azores high pressure center and the presence of a low pressure system over the Mediterranean sea will therefore produce a positive contribution to the first main mode of variation. This synoptic pattern is responsible for northwestern circulations over the CFN (Jiménez et al. 2009a) in agreement with the surface flow structure of the first EOF (Fig. 3). The anticyclonic circulations over the Atlantic introduce northern winds over the Iberian Peninsula which turn to northwestern winds over the area of study due to the channeling of the flow between the main mountain systems in northern Iberia and the effects of the surface friction and the associated ageostrophic balance (Jiménez et al. 2009a).

The second mode shows a negative correlation center to the south of the British Islands, and a weaker positive one over western Africa (Fig. 7b). Hence, the synoptic pattern related to the positive phase of the second main mode of variation is associated with the presence of a low pressure system to the north of the CFN and a reinforcement of the Azores high pressure over Africa. This pressure configuration introduces western geostrophic circulations over the CFN which turn to southwestern ones close to the surface due to the ageostrophic balance introduced by the surface friction (Jiménez et al. 2009a). This coincides with the main direction of the flow in the second EOF (Fig. 4).

Additional support to the previous interpretations is obtained by analysing the periods showing the maximum anomalies in the PCs (Fig. 5). PC1 shows the maximum value on 26 December 1980 and the minimum negative value on 9 December 1989 whereas PC2 shows the maximum positive value on 6 December 1965 and the negative one on 25 February 1993 (Fig. 5).The averaged anomalies of the wind and SLP fields over the periods centered on these maximum values and including 30 days before and after in order to mimic the filtering of the moving average used in Fig. 5 are shown in Fig. 8. The anomalies are in

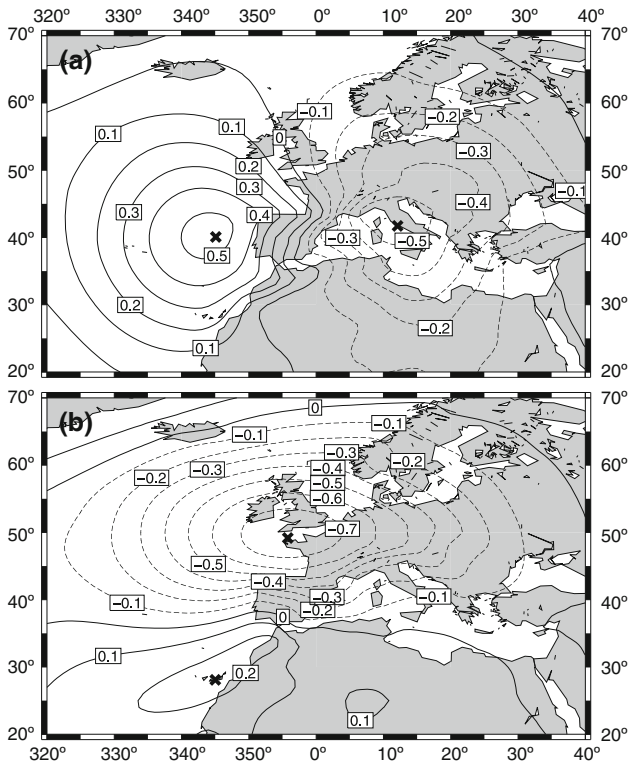

Fig. 7 Correlation map between the SLP from the ECMWF datasets (ERA-40 before August 2002 and the operational analysis afterwards) and the PC1 (**a**) and PC2 (**b**). The *crosses* represent the locations used to calculate the Index 1 (**a**) and the Index 2 (see Sect. 4.2) (**b**)

concordance with the structure of the correlation maps shown in Fig. 7. The maximum in PC1 shows a zonal pressure gradient (Fig. 8a) that introduces northwestern circulations into the CFN whereas the minimum shows the opposite pressure configuration and it is responsible for southeastern regional winds (Fig. 8b). The NW-SE circulations are in concordance with the wind circulations associated with the first EOF (Fig. 3). The SLP anomalies associated with the maximum and minimum of PC2 show a meridional pressure gradient (Fig. 8c, d). The maximum is responsible for southwestern wind anomalies (Fig. 8c) whereas the minimum introduces northeastern winds over the CFN (Fig. 8d) in agreement with the SW–NE orientation of the flow in the second EOF (Fig. 4).

Complementary information supporting the previous interpretations is provided by the classification of daily SLP fields over the Iberian Peninsula into its most frequent pressure patterns (PPs) identified in Jiménez et al. (2009a). The classification was performed using SLP information during the observational period (1992–2005). PCA was applied to the correlation matrix of the SLP fields before using a two step cluster analysis procedure to identify the PPs. Briefly, the PPs identified are associated with a displacement of the Azores High towards the British Islands (PP1); the Azores High modulated by low pressures over Europe (PP2); a low pressure system coming from the polar front (PP3), the Iberian thermal low (PP4); a pattern with a meridional orientation of the Azores high and a low pressure center in the Mediterranean sea (PP5); the influence of the high pressures of the Siberian high (PP6); a NE extension of the Azores high over the Iberian Peninsula and Europe (PP7); and anticyclonic situations over both the Atlantic and Mediterranean sea (PP8).

The classification has been herein extended to the 1960–2005 period by assigning the SLP fields from 1960 to 1991 to its most similar PP. For this purpose, the normalized SLP fields were assigned to the most similar centroid of each PP. Then, the relative frequency of appearance of each one of the eight PPs during each year is computed and correlated with the yearly averaged time series of the PCs. The two PPs that show the highest correlation with PC1 and PC2 are shown in Fig. 9a–d, respectively.

PP5 contributes to the positive phase of the first mode of variation ($r = 0.57$) whereas PP6 to the negative one ($r = -0.76$). The anomalies of PP5 show a positive center over the Atlantic ocean and a negative one over the Mediterranean sea (Fig. 9a). The pattern is therefore similar to the correlation map of PC1 (Fig. 7a) but shows a certain clockwise rotation. It is responsible for northwestern anomalous circulations over the region (Fig. 9a). PP6 shows negative pressure anomalies over the Atlantic ocean and positive ones over Europe that are responsible for the southeastern anomalies over the region (Fig. 9b). This NW-SE direction of the flow introduced by these PPs is in agreement with the surface circulations shown by the first EOF (Fig. 3). The anomalies in PP5 are generated by the reinforcement of the Azores High that shows a certain meridional extension, and the presence of low pressures in the Mediterranean sea whereas the anomalies of PP6 are associated with the presence of a continental high pressure over Europe (Jiménez et al. 2009a).

The PPs showing the highest correlation with PC2 are PP1 ($r = -0.59$) and PP3 ($r = 0.60$). PP1 is associated with positive anomalies over the British Islands (Fig. 9c) whereas PP3 shows negative ones (Fig. 9d). The PPs show the SW–NE direction of the flow over the CFN in agreement with the circulations shown by the second EOF (Fig. 4). Physically, these anomalies are created by the displacement of the Azores high pressure system towards the British Islands or the presence of a low pressure system over the Atlantic ocean (Jiménez et al. 2009a).

4.2 Climate indexes

The previous results suggest that the surface wind variability over the CFN can be represented by two indexes calculated with the SLP differences between the positive and negative correlation centers (Fig. 7). Index 1 is defined

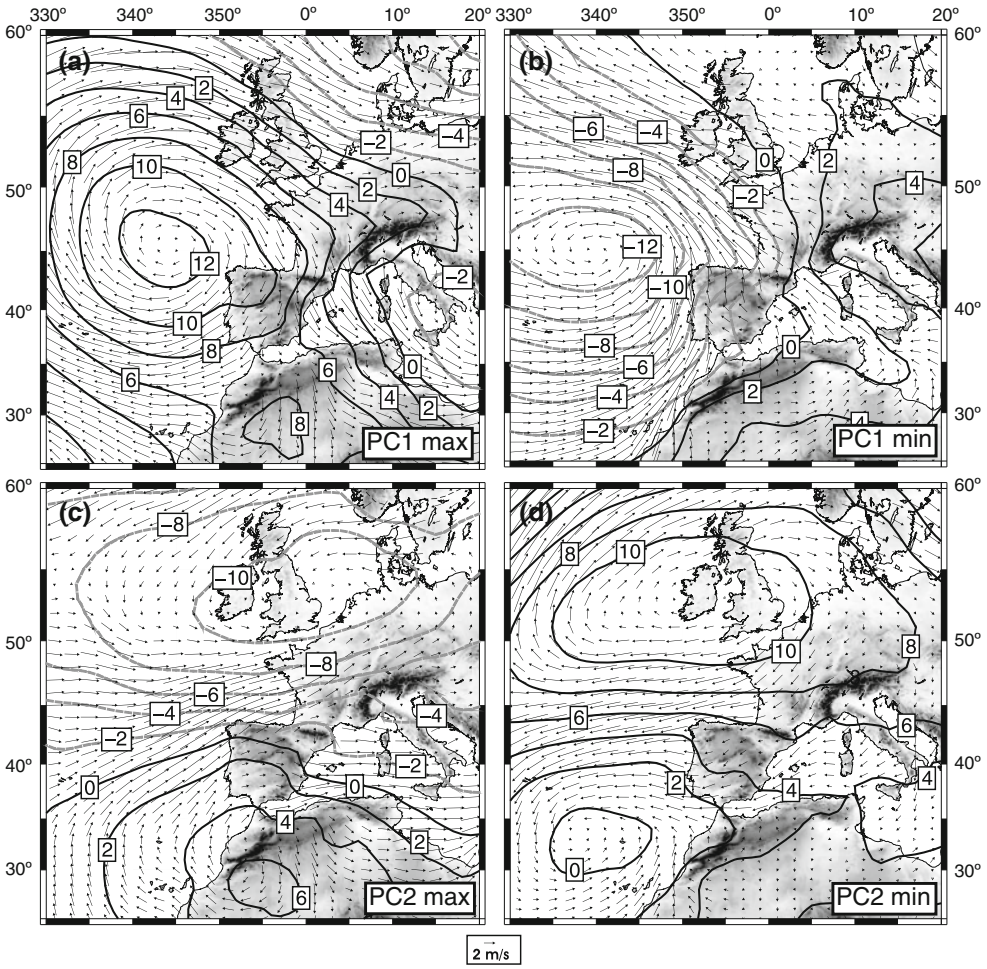

Fig. 8 Anomalies of the wind and SLP for the periods with the maximum and minimum values of PC1 (**a**, **b**) and PC2 (**c**, **d**)

as the pressure at 40 N 15 W minus the pressure at 42 N 12 E (crosses in Fig. 7a), whereas Index 2 is defined as the pressure at 49 N 4 W minus pressure at 28 N 15 W (crosses in Fig. 7b). It should be noted that the first index represents a zonal pressure gradient (Fig. 7a) whereas the second one represents a more meridional one (Fig. 7b). As expected, Index 1 is correlated with the first PC ($r = 0.82$) and Index 2 with the second PC ($r = -0.82$).

To illustrate the importance of this finding, the relationship of the large scale pressure gradients (Index 1 and Index 2) and the regional wind variability (the PCs) is compared to the one obtained using the main teleconnection patterns in the North Atlantic area: the North Atlantic Oscillation index (NAO), the East Atlantic pattern (EA), East Atlantic/Western Russia (EA/WR) pattern and the Scandinavian pattern (SCA). The teleconnection patterns represent preferred modes of the planetary scale circulation that can be expected to condition the climate fluctuations at the surface (Barnston and Livezey 1987). Indeed, important associations between these patterns and temperature and precipitation anomalies over Europe have been identified (e.g. Hurrell 1995). The NAO shows a north-south dipole with negative anomalies over Greenland and positive in the central latitudes of the North Atlantic ocean in its positive phase. The EA shows a similar pattern to NAO but with the dipole displaced southeastward. The EA/WR consist of four anomaly centers, the positive phase is characterized by two positive centers in western Europe and northern China and negative ones in the central North Atlantic ocean and eastern Russia. Finally, the SCA shows anticyclonic (cyclonic) conditions in Scandinavia in its positive (negative) phase. The climate indexes were calculated according with Barnston and Livezey (1987). Since the teleconnection indexes are defined on a monthly basis, the correlation of the PCs and the SLP has also been calculated at monthly time scales. The comparison is shown in Table 3.

There are significant correlations between the climate indexes and the PCs, with a maximum value of 0.41 for the EA pattern and the PC2. This association can be understood in terms of the similarity between the positive phase of EA, low pressure center in central Atlantic and positive anomalies to the southeast, and the anomaly pattern associated with the second mode of variation (Fig. 7b). However, EA also shows significant correlation with the first PC ($r = 0.26$). Thus, it can be said that the EA mode presents

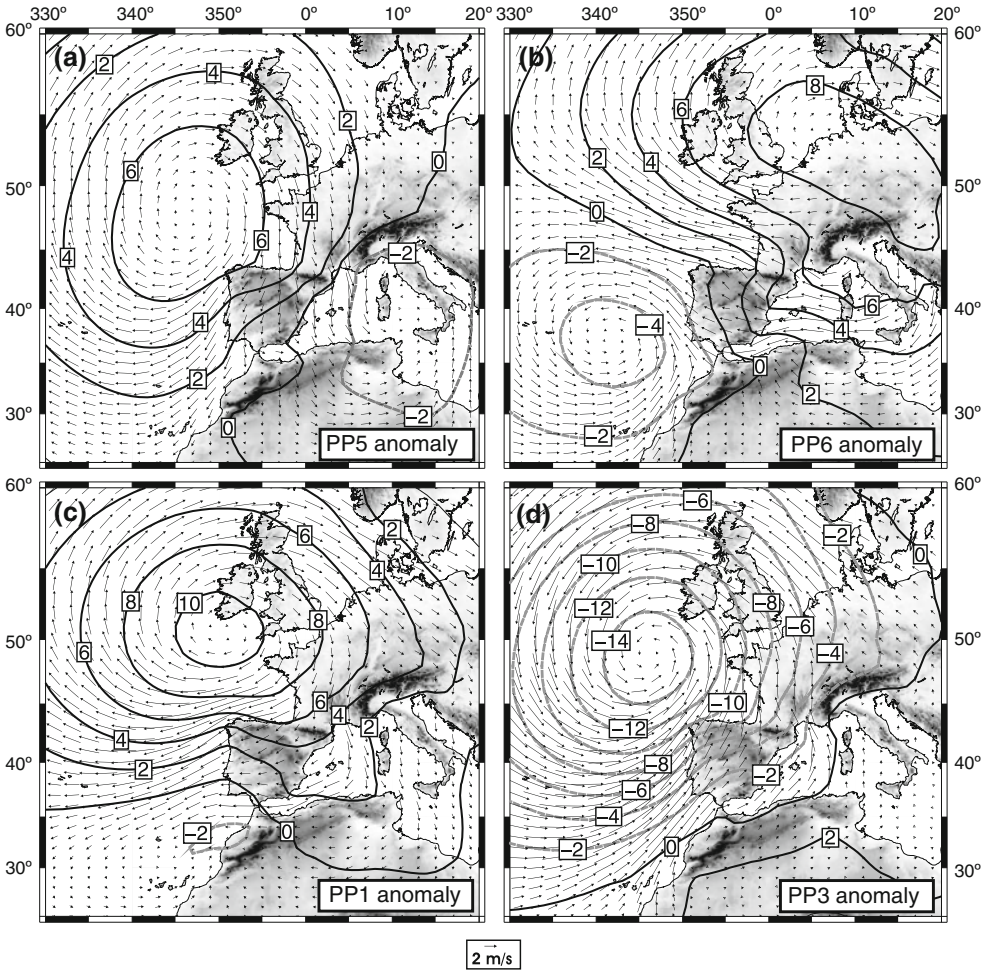

Fig. 9 Anomalies of the wind and SLP for the days classified as PP5 (**a**), PP6 (**b**), PP1 (**c**) and PP3 (**d**) during the period from 1960 to 2005. Data from the ECMWF dataset used as initial and boundary conditions for the WRF simulation are used

Table 3 Correlations of monthly averaged PCs with Index 1 and Index 2 (see Sect. 4.2) and relevant teleconnection indexes in the North Atlantic (Barnston and Livezey 1987)

	Index 1	Index 2	NAO	EA	EA/WR	SCA
PC1	**0.91**	−0.03	0.06	**−0.26**	**−0.28**	0.02
PC2	−0.06	**−0.90**	**−0.23**	**0.41**	**−0.17**	**0.27**

Significant correlations at the 5% level are shown in bold

contributions to both PCs of the surface wind. Although with smaller correlation values, the EA/WR series is also correlated to some degree with the first (r = 0.26) and the second (r = −0.17) PCs. The positive anomalies in western Europe, and the negative ones in Russia, contribute to the positive phase of the first mode (Fig. 7a); and to a lesser extent to the negative phase of the second one. SCA and NAO show significant correlations just with PC2, but the correlation values are quite modest (r = 0.27 and r = −0.23, respectively). Both, the positive phase of NAO and the negative one of SCA are associated with negative anomalies in northern Europe which certain resemblances to the anomaly pattern responsible for the variability of the second mode (Fig. 7b). Similar modest associations were found using the canonical series from the lower troposphere structure and the regional wind during an extended winter season by García-Bustamante et al. (2012).

The associations between the PCs and the indexes of the synoptic pressure gradients are much higher (Table 3). The first (second) PC, associated with the zonal (meridional) index, shows a correlation of 0.91 (−0.90). The high correlation is expected given the definition of the indexes. The interesting thing is that the large scale pressure gradients are more suitable to describe the wind variability over the CFN than the most important teleconnection patterns over the North Atlantic region.

The large associations found between the two indexes representing the zonal and meridional pressure gradients (Fig. 7) and the surface wind variability allow to use information of the SLP fields to further inspect the regional wind variability in absence of observations or even numerical simulations. For instance, SLP observations from the instrumental period can be used to explore the wind variability before 1960 when the WRF downscaling is not available. This is further illustrated using SLP

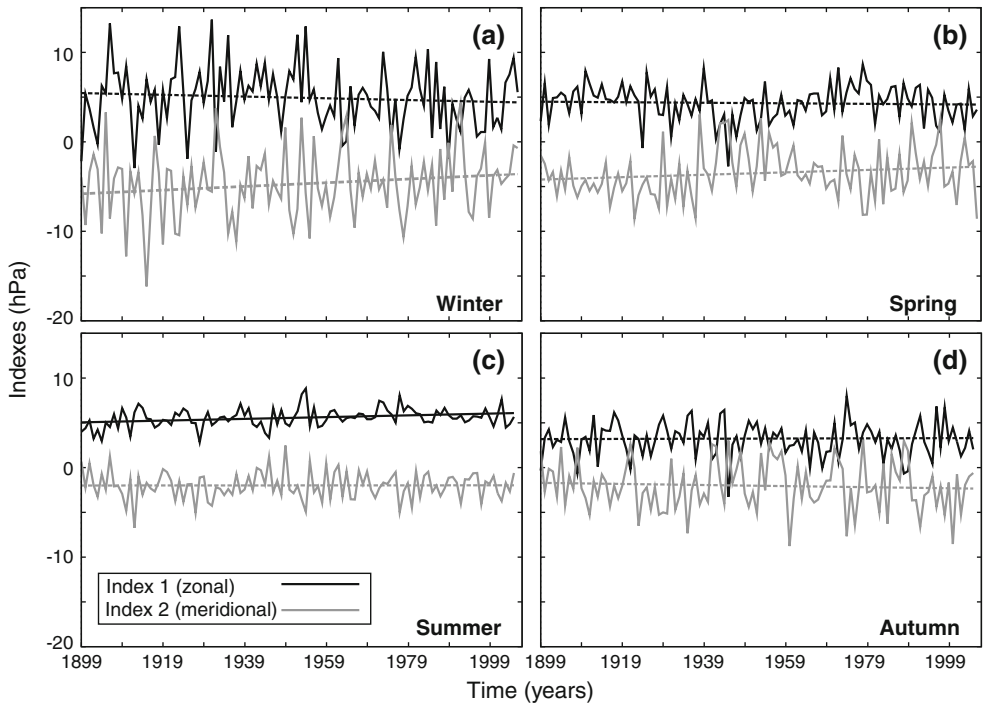

Fig. 10 Time series of the Index 1 (*black*) and the Index 2 (*gray*) during each season: winter (**a**), spring (**b**), summer (**c**) and autumn (**d**). The *straight lines* represent the trends of the time series which are solid if they are statistically significant at the 5% level according to the Mann–Kendall test

observations during the 1899–2006 period (Trenberth and Paolino 1980) to inspect potential trends of the wind during the last century (Fig. 10). The Mann–Kendall trend test (Mann 1945; Kendall and Gibbons 1990) is used to detect the significant trends. The analysis is split for each season in order to discriminate between the different synoptic contributions dominant during each of them. The meridional gradient shows positive trends during Winter and Spring, and negative trends during Summer and Autumn, but all of them are non-significant. The zonal gradient shows less important trends but there is a significant one towards an increment of the zonal gradient in Summer (Fig. 10c). This behavior points to an increase of the positive phase of the first mode of variation (Fig. 3) which favors the intensification of the northwestern circulations.

5 Summary and conclusions

A dynamical downscaling performed with the WRF model has been used to complement the wind information provided by a mesoscale network over the CFN, a complex terrain region in the northeast of the Iberian Peninsula. The simulation's ability to reproduce the wind variability during the observational period (1992–2005, JEA10a) motivated its extension in this work (1960–2005) in order to investigate the wind behavior where and when observations are not available and provide a statistically robust characterization of the main synoptic mechanisms responsible for the regional variability. The investigation focuses on daily time scales in order to analyze the influence that the large scale interaction with topography exerts over the surface circulations. Further research will be oriented to understand the wind variability at smaller atmospheric scales in order to investigate the contributions of the mesoscale circulations (e.g. Jiménez et al. 2011). The wind variability was inspected using PCA applied to the joint correlation matrix of the surface wind components.

The first principal mode of variation reflects the channeling of the flow between the large mountain systems in northern Iberia and the modulation exerted by the smaller topographic features of the CFN. The second mode reveals a differentiated wind behavior between the mountains areas and the valleys. In spite of certain wind speed biases evidenced in the downscaling (see Jiménez and Dudhia 2012), the high horizontal resolution used allowed to identify, for instance, the main areas that connect the flow from the north of the CFN with those over the Ebro valley in the South. This finding illustrates the kind of complementary information that a downscaling at high horizontal resolution provides to purely observational investigations where the spatial sampling of the wind is more limited

(e.g. JEA08). In this sense, results from this numerical simulation can be used in the future to provide further understanding of the transport and dispersion of pollutants along the region from the industrial areas in the coast (e.g. Millán et al. 1991). Additionally, the simulation can help to analyze the sustainability of the numerous wind farms installed over the region (Fairless 2007; García-Bustamante et al. 2008, 2009). The long temporal period covered by the simulation can be used to provide information of the long-term variability of the wind at the location of the already installed wind farms, and thus inform us about the sustainability of the electricity generated from the wind.

The downscaling showed particularly good agreement with observations in the reproduction of the temporal wind variability. Both modes show significant contributions at the highest frequencies (fewer than 10 days) with different contributions at lower ones. A tendency to increase the significant contributions of periods between 100 and 500 days (about 2 years) was noticed in the NW–SE circulations of the first EOF. The investigation revealed a small contribution of the decadal variability, result that go further beyond to the previous observational and modeling studies over the area (JEA08, JEA10a) that focused on a shorter temporal period (1992–2005).

An important finding of this investigation is the strong influence that the zonal and meridional synoptic pressure gradients exert over the surface wind variability. High pressures over the Atlantic ocean and negative ones in the north of Italy contribute to the positive phase of the first mode of variation; whereas high pressures to the south of the British Islands and negative ones over western Africa reinforce the positive phase of the second mode. These important findings were used to study the trends in the wind variability during the last century. Hence, results from the WRF downscaling were used to go even further than what is directly allowed for the temporal coverage of the downscaling. A significant increase of the northwestern wind anomalies during Summer becomes evident. The use of SLP fields from climate change projections for investigating potential changes of the regional surface wind variability constitutes an interesting topic for future research.

Acknowledgments This investigation was partially supported by projects CGL-2008-05093/CLI, CGL-2011-29677-C02, and PSE-120000-2008-9 and was accomplished within the collaboration agreement 09/153 between CIEMAT and UCM as well as the collaboration agreement 09/490 between CIEMAT and NCAR. NCAR is sponsored by the National Science Foundation. We would like to thank the Navarra Government and the ECMWF for facilitating the access to their data sets. We also would like to thank the reviewers for their comments which helped to improve the quality of the original manuscript. An initial version of the wavelet software was provided by C. Torrence and G. Compo (available on line at http://atoc.colorado.edu/research/wavelets/).

References

Archer CL, Jacobson MZ (2003) Spatial and temporal distributions of U.S. winds and wind power at 80 m derived from measurements. J Geophys Res 108(D9):4289. doi:10.1029/2002JD002076

Archer CL, Jacobson MZ (2004) Correction to "Spatial and temporal distributions of U.S. winds and wind power at 80 m derived from measurements". J Geophys Res 109:D20116. doi:10.1029/2004JD005099

Barnston AG, Livezey RE (1987) Classification, seasonality and persistence of low-frequency atmospheric circulation patterns. Mon Weather Rev 115:1083–1126

Buckley RL (2004) Statistical comparison of Regional Atmospheric Modelling System forecasts with observations. Meteorol Appl 11:67–82

Burlando M, Antonelli M, Ratto CF (2008) Mesoscale wind climate analysis: identification of anemological regions and wind regimes. Int J Climatol 28:629–641

Davy R, Woods M, Russell C, Coppin P (2010) Statistical downscaling of wind variability from meteorological fields. Bound Layer Meteorol 135(1):161–175

Fairless D (2007) How did a little Spanish province become one of the world's wind-energy giants? Nature 447:1046–1048

García-Bustamante E, González-Rouco JF, Jiménez PA, Navarro J, Montávez JP (2008) The influence of the Weibull assumption in monthly wind energy estimation. Wind Energy 11:483–502

García-Bustamante E, González-Rouco JF, Jiménez PA, Navarro J, Montávez JP (2009) A comparison of methodologies for monthly wind energy estimations. Wind Energy 12:640–659

García-Bustamante E, González-Rouco JF, Navarro J, Xoplaki E, Jiménez PA, Montávez JP (2012) North Atlantic atmospheric circulation and surface wind in the Northeast of the Iberian Peninsula: uncertainty and long term downscaled variability. Clim Dyn 38:141–160

George SS, Wolfe SA (2009) El Niño stills winter winds across the southern Canadian Prairies. Geophys Res Lett 36:L23806. doi:10.1029/2009GL041282

Guo H, Xu M, Hu Q (2011) Changes in near-surface wind speed in China: 1969–2005. Int J Climatol 31:349–358

He Y, Monahan AH, Jones CG, Dai A, Biner S, Caya D, Winger K (2010) Probability distributions of land surface wind speeds over North America. J Geophys Res 115:D04103. doi:10.1029/2008JD010708

Horel J, Splitt M, Dunn L, Pechmann J, White B, Ciliberti C, Lazarus S, Slemmer J, Zaff D, Burks J (2002) Mesowest: cooperative mesonets in the western United States. Bull Am Meteorol Soc 83:211–225

Hughes M, Hall A (2010) Local and synoptic mechanisms causing Southern California's Santa Ana winds. Clim Dyn 34(6):847–857

Hurrell JW (1995) Decadal trends in the north atlantic oscillation: Regional temperatures and precipitation. Science 269:676–679

Jiménez PA, Dudhia J (2012) Improving the representation of resolved and unresolved topographic effects on surface wind in the WRF model. J Appl Meteorol Climatol 51:300–316

Jiménez PA, González-Rouco JF, Montávez JP, Navarro J, García-Bustamante E, Valero F (2008) Surface wind regionalization in complex terrain. J Appl Meteorol Climatol 47:308–325

Jiménez PA, González-Rouco JF, Montávez JP, García-Bustamante E, Navarro J (2009a) Climatology of wind patterns in the northeast of the Iberian Peninsula. Int J Climatol 29:501–525

Jiménez PA, Montávez JP, García-Bustamante E, Navarro J, Jiménez-Gutiérrez JM, Lucio-Eceiza EE, González-Rouco JF (2009b) Diurnal surface wind variations over complex terrain. Física de la Tierra 21:79–91

Jiménez PA, González-Rouco JF, García-Bustamante E, Navarro J, Montávez JP, Vilà-Gueraude Arellano J, Dudhia J, Roldán A (2010a) Surface wind regionalization over complex terrain: evaluation and analysis of a high resolution WRF numerical simulation. J Appl Meteorol Climatol 49:268–287

Jiménez PA, González-Rouco JF, Navarro J, Montávez JP, García-Bustamante E (2010b) Quality assurance of surface wind observations from automated weather stations. J Atmos Ocean Technol 27:1101–1122

Jiménez PA, Vilà-Gueraude Arellano J, González-Rouco JF, Navarro J, Montàvez JP, García-Bustamante E, Dudhia J (2011) The effect of heatwaves and drought on the surface wind circulations in the NE of the Iberian Peninsula during the summer of 2003. J Clim 24:5416–5422

Kalnay E et al (1996) The NCEP/NCAR 40 year reanalysis project. Bull Am Meteorol Soc 77:437–471

Kaufmann P, Weber RO (1996) Classification of mesoscale wind fields in the MISTRAL field experiment. J Appl Meteorol 35: 1963–1979

Kaufmann P, Whiteman CD (1999) Cluster-analysis classification of wintertime wind patterns in the Grand Canyon region. J Appl Meteorol 38:1131–1147

Kendall MG, Gibbons JD (1990) Rank correlation methods, 5th edn. Griffin, London

Klink K (1999) Trends in mean monthly maximum and minimum surface wind speeds in the coterminous United States, 1961 to 1990. Clim Res 13:193–205

Klink K (2002) Trends and interannual variability of wind speed distributions in Minnesota. J Clim 15:3311–3317

Klink K (2007) Atmospheric circulation effects on wind speed variability at turbine height. J Appl Meteorol Climatol 46: 445–456

Lo JCF, Yang ZL, Pielke RA Sr (2008) Assessment of three dynamical climate downscaling methods using the Weather Research and Forecasting (WRF) model. J Geophys Res 113: D09112

Ludwig FL, Horel J, Whiteman CD (2004) Using EOF analysis to identify important surface winds patterns in mountain valleys. J Appl Meteorol 43:969–983

Mann HB (1945) Nonparametric tests against trend. Econometrica 13:245–259

Martín M, Valero F, Morata A, Luna M, Pascual A, Santos-Muñoz D (2011) Springtime coupled modes of regional wind in the Iberian Peninsula and large-scale variability patterns. Int J Climatol 31: 880–895

McVicar TR, Van Niel TG, Li LT, Roderick ML, Rayner DP, Ricciardulli L, Donohue RJ (2008) Wind speed climatology and trends for Australia, 1975–2006: capturing the stilling phenomenon and comparison with near-surface reanalysis output. Geophys Res Lett 35:L20403. doi:10.1029/2008GL035627

McVicar T, Van Niel T, Roderick M, Li L, Mo X, Zimmermann N, Schmatz D (2010) Observational evidence from two mountainous regions that near-surface wind speeds are declining more rapidly at higher elevations than lower elevations: 1960–2006. Geophys Res Lett 37(6):L06402

Millàn MM, nano BA, Alonso L, Navazo M (1991) The effect of meso-scale flows on regional and long-range atmospheric transport in the western Mediterranean area. Atmos Environ 25: 949–963

PaiMazumder D, Mölders N (2009) Theoretical assessment of uncertainty in regional averages due to network density and design. J Appl Meteorol Climatol 48(8):1643–1666

Palutikof JP, Kelly PM, Davies TD, Halliday JA (1987) Impacts of spatial and temporal wind speed variability on wind energy output. J Appl Meteorol 26:1124–1133

Pryor SC, Barthelmie RJ (2003) Long-term trends in near-surface flow over the Baltic. Int J Climatol 23:271–289

Pryor SC, Ledolter J (2010) Addendum to "Wind speed trends over the contiguous United States". J Geophys Res 115:D10103. doi: 10.1029/2009JD013281

Pryor SC, Barthelmie RJ, Young DT, Takle ES, Arritt RW, Flory D, Gutowski WJ Jr, Numes A, Roads J (2009) Wind speed trends over the contiguous United States. J Geophys Res 114:D14105

Rahimzadeh F, Noorian A, Pedram M, Kruk M (2011) Wind speed variability over Iran and its impact on wind power potential: a case study for Esfehan Province. Meteorol Appl 18:198–210

Rife DR, Davis CA (2005) Verification of temporal variations in mesoscale numerical wind forecast. Mon Weather Rev 133: 3368–3381

Rife DR, Davis CA, Liu Y, Warner TT (2004) Predictability of low-level winds by mesoscale meteorological models. Mon Weather Rev 132:2533–2569

Rife D, Davis C, Knievel J (2009) Temporal changes in wind as objects for evaluating mesoscale numerical weather prediction. Wea Forecasting 24(5):1374–1389

Skamarock WC, Klemp JB, Dudhia J, Gill DO, Barker DM, Wang W, Powers JG (2005) A description of the advanced research WRF Version 2. Tech. Rep. TN-468+STR, NCAR

Torrence C, Compo GP (1998) A practical guide to wavelet analysis. Bull Am Meteorol Soc 79:61–78

Trenberth KE, Paolino DA (1980) The northern hemispheric sea-level pressure data set: trends, errors and discontinuities. Mon Weather Rev 108:855–872

Uppala SM, Kallberg PW, Simmons AJ, Andrae U, da Costa Bechtold V, Fiorino M, Gibson JK, Haseler J, Hernandez A, Kelly GA, Li X, Onogi K, Saarinen S, Sokka N, Allan RP, Andersson E, Arpe K, Balmaseda MA, Beljaars A, van de Berg L, Bidlot J, Bormann N, Caires S, Chevallier F, Dethof A, Dragosavac M, Fisher M, Fuentes M, Hagemann S, Holm E, Hoskins BJ, Isaksen L, Janssen P, Jenne R, McNally AP, Mahfouf J, Morcrette J, Rayner NA, Saunders RW, Simon P, Sterl A, Trenberth KE, Untch A, Vasiljevic D, Viterbo P, Woollen J (2005) The era-40 re-analysis. Q J R Meteorol Soc 131:2961–3012

Vautard R, Cattiaux J, Yiou P, Thépaut J, Ciais P (2010) Northern Hemisphere atmospheric stilling partly attributed to an increase in surface roughness. Nat Geosci 3(11):756–761

Wan H, Wang X, Swail V (2010) Homogenization and trend analysis of Canadian near-surface wind speeds. J Clim 23(5):1209–1225

Xu M, Chang CP, Fu C, Qi Y, Robock A, Robinson D, Zhang H (2006) Steady decline of east Asian monsoon winds, 1969–2000: evidence from direct ground measurements of wind speed. J Geophys Res 111:D24111. doi:10.1029/2006JD007337

Zagar N, Zagar M, Cedilnik J, Gregoric G, Rakovec J (2006) Validation of mesoscale low-level winds obtained by dynamical downscaling of ERA40 over complex terrain. Tellus 58:445–455